

A Wideband Envelope Modulator Design for Envelope-Tracking SiGe Power Amplifier (ET-PA) for Broadband Wireless Applications

Yan Li⁺, Jerry Lopez^{*+}, and Donald Y.C. Lie⁺

RF Micro Devices Inc., Phoenix, AZ, USA

^{*}NoiseFigure Research Inc., Lubbock, TX, USA

⁺Department of Electrical and Computer Engineering

Texas Tech University, Lubbock, TX, USA

e-mail: donald.lie@ttu.edu

Abstract — This work presents a design example of a wideband envelope modulator (EM) that can effectively modulate the instantaneous supply voltage for a monolithic SiGe power amplifier to form a highly efficient envelope-tracking power amplifier (ET-PA) system for potential broadband wireless applications. Trade-offs between linearity, switching noise, efficiency and bandwidth have been examined carefully with both experimental data and RF/analog/digital co-simulations. The SiGe ET-PA using our wideband EM was characterized by the WiMAX 64QAM 8.75 MHz signal, showing an overall PAE of 30.5% at output power of 17 dBm with an error vector magnitude (EVM) of 4.4%, while successfully passing the stringent WiMAX spectral mask.

Keywords: Broadband wireless; envelope modulator; envelope-tracking (ET); LTE; SiGe; power amplifier (PA); WiMAX

I. INTRODUCTION

Recently, envelope-tracking (ET) has become a very popular efficiency enhancement technique for RF power amplifiers (PAs) design [1]-[5]. Split-band design concept has been applied to the envelope modulator (EM) for wideband applications [1] [4] [5]. However, compared with narrowband cellular applications (e.g., EDGE), the high peak-to-average power ratio (PAPR or PAR) of the broadband signals (e.g., LTE/WiMAX) require the EM to have wider bandwidth and lower distortion, while still maintaining excellent efficiency. Therefore, careful investigations of the design trade-offs for the wideband EM are still required. In this paper, we will report a design example for a wideband EM paired with a SiGe monolithic PA to form an effective ET-PA system for potential broadband wireless applications. A discrete linear-assisted switching EM is designed to investigate the overall ET-PA system performances by experimental data and RF/analog/digital co-simulation. The effects of bandwidth and switching frequency as two major factors on linearity and efficiency will be studied carefully to make this EM applicable for high PAR wideband applications.

This paper is organized as follows. Section II presents the designs of the common-emitter SiGe PA and linear-assisted switching EM. In Section III, we demonstrate the effective of our designed EM by applying it to the SiGe PA to form an ET-PA system. A WiMAX 64QAM 8.75 MHz signal (PAR of 10.5 dB) will be applied to the ET-PA to

showcase the efficiency and linearity enhancements of the ET technique over traditional fixed-supply PAs.

II. CIRCUITS DESIGN

A. Design of Common-Emitter SiGe Power Amplifier

A monolithic 1-stage common-emitter SiGe PA is used here as an example to form an ET-PA system to study the trade-offs for wideband EM design. This PA was designed and fabricated in IBM 7HP 0.18 μ m SiGe BiCMOS technology [1]-[3]. The simplified schematic and die picture of the PA are shown in Fig. 1. The high-breakdown heterojunction bipolar transistor (HBT) option is used for the PA design with a total emitter-area of 220 μ m² (typical $BV_{CEO}=4.2$ V; $BV_{CBO}=12.5$ V). This monolithic SiGe PA was tested on a FR4 PCB. The RF Choke (RFC) inductor was left off-chip to achieve high Q at 2.4 GHz for better power-added-efficiency (PAE). A high-Q bondwire is used as the output tank inductor design, together with more than 4 downbonds (i.e., bondwires at the emitter node) to reduce the ground parasitic inductance for high PAE [3]. No other off-chip elements are needed nor used for the PA input and output matching.

It is important to characterize the PA thoroughly before designing the EM for optimal ET-PA performances, as the collector impedance presented by the PA (R_{load}) will affect the efficiency and linearity performance of the EM. Fig. 2 shows the measured PAE vs. output power (P_{out}) at different supply voltage V_{CC} in the continuous wave (CW) mode. For the fixed-supply PA, its PAE reduces rapidly when P_{out} drops, but the PAE at low P_{out} can be greatly enhanced by varying V_{CC} as shown by the dash curve, which shows the idea for an ET-PA operation. The dash curve is obtained at each peak PAE point of different V_{CC} levels. This characteristic of PAE enhancement indicates that the ET technique can improve the average efficiency of the PA compared with the case of a fixed-supply PA. Fig. 2 also plots the collector impedance presented by the PA to the EM (i.e., R_{load}), which is calculated from the DC supply voltage and the measured DC supply current of the PA at each peak PAE point (please refer to Fig. 4 for the definition of R_{load} [4]). The R_{load} presented by the PA varies, dependent on the operating regions of the PA [1]. According to the measurement data shown in Fig. 2, R_{load} can change roughly from 70 Ω to 10 Ω when P_{out} increases from 8 dBm to 20 dBm.

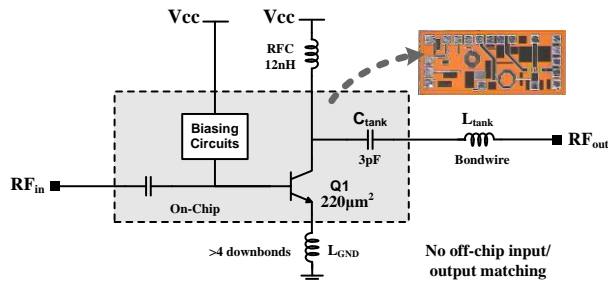


Fig. 1 Simplified schematic and die picture of the 1-stage PA designed and fabricated in IBM 7HP 0.18 μm SiGe BiCMOS technology

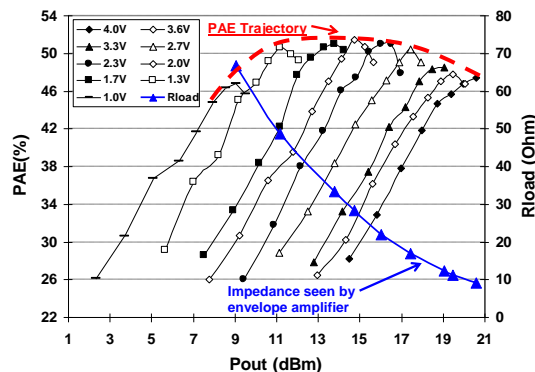


Fig. 2 Measured PAE vs. P_{out} of the SiGe PA, and the impedance seen by the EM by changing the PA supply voltage (V_{CC}) biasing in the CW mode

B. Linear-Assisted Switching Envelope Modulator

A proper EM design is critical to achieve the best overall efficiency and linearity performances for an ET-PA. As reported in [1]-[4], the finite bandwidth and the associated group delay of the EM are large contributors of nonlinearity in an ET-PA. In addition, to take advantage of the efficiency enhancement provided by the ET technique, the EM needs to maintain high efficiency throughout the ET-PA operation. The overall power efficiency of an ET-PA system is the product of the EM efficiency and the PA collector efficiency (CE), which is expressed as:

$$\eta_{\text{ET-PA}} = \eta_{\text{Env.-Mod.}} \cdot \eta_{\text{PA,CE}} \quad (1)$$

Therefore, the EM design targets are high efficiency and wide bandwidth to track the instantaneous input envelope.

1) Split-Band Design of the Envelope Modulator

The envelope signal is extracted from the modulated I/Q (i.e., in-phase/quad-phase) signals from the LTE/WiMAX baseband and then feed into the EM. Such nonlinear transformation will expand the bandwidth of the envelope by a factor of 5-10 compared with the original signal bandwidth [4] [5]. Conventionally, the EM can be implemented in the form of a linear regulator (e.g., a low dropout regulator (LDO) as in [6]), as the linear topology offers wide bandwidth and can be with almost no output ripple. Nonetheless, the power efficiency of linear regulator is very poor when the output voltage level is low [6], making it unsuitable for high PAR signals for 3G/4G

applications. On the other hand, a switching regulator has high power efficiency across a broad range of output voltage, but it produces significant output ripples and its bandwidth is constrained to be a fraction of the switching frequency [7], making it suitable only for narrowband applications such as the North American Digital Cellular (NADC) in [7]. Switching regulators can also be applied to high data-rate systems when a rather high switching frequency is employed [8], but the high switching frequency inevitably causes high switching loss that limits the power efficiency (e.g., $\sim 76\%$ maximum for WCDMA in [8]) and also can degrade ET-PA linearity considerably, which can often defeat the purpose of using switching regulators.

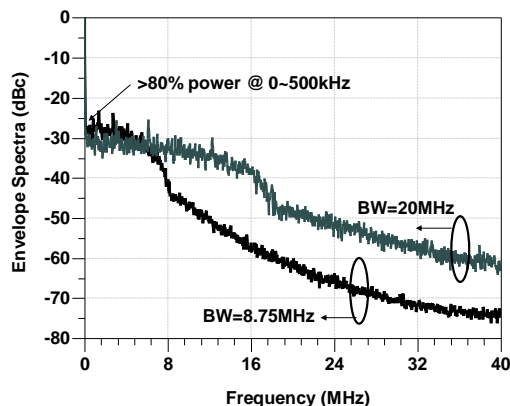


Fig. 3 Simulated envelope spectra of WiMAX 8.75/20 MHz signals.

Many recent reports on the wideband EM design for ET-PA have combined the advantages of a wideband linear regulator and a high efficiency switching regulator in various ways [9]-[11]. Fig. 3 shows the simulated envelope spectra of WiMAX 8.75 MHz and 20 MHz signals (PAR of ~ 10.2 dB). An important characteristic of the envelope spectrum is that $\sim 80\%$ of envelope power resides from DC to several kHz, while over 99% of the envelope power resides within DC to 8MHz for the 8.75 MHz signal, and within DC to 20 MHz for the 20 MHz signal, respectively. Such a characteristic of the envelope spectrum implies that a “split-band” EM design (or often called “linear-assisted switching” structure) can achieve a high efficiency over a wide bandwidth [4]. The split-band EM consists of a wideband linear stage (therefore of low efficiency) and a high efficiency narrowband switching stage. This split-band design lessens the requirements of the switching stage, since the fast transients of the envelope signal will be taken care of by the wideband linear stage, while the switching stage will handle DC and the slow moving signals with high efficiency. The efficiency of the entire EM ($\eta_{\text{env.-mod.}}$) is a combination of the switching stage efficiency (η_{SW}) and the linear stage efficiency (η_{lin}), as expressed by:

$$\frac{1}{\eta_{\text{env.-mod.}}} = \frac{\alpha}{\eta_{\text{SW}}} + \frac{1-\alpha}{\eta_{\text{lin}}} \quad (2)$$

, where α is the ratio of the output power from the switching stage to the total output power of the EM [4] [12].

2) Discrete Envelope Modulator Design

The linear-assisted switching EM is designed by using commercial-of-the-shelf (COTS) components to investigate the overall efficiency and linearity trade-off in an ET-PA system. Fig. 4 shows the circuit implementation of the discrete EM using an operational amplifier (Op-Amp) as the linear stage and a buck converter as the switching stage. The buck converter supplies the slow slew-rate load current (I_{SW}) that contributes to the majority of the load current (I_{load}) to ensure high efficiency, while the wideband linear Op-Amp stage operates in a feedback mode to track the high slew-rate current (I_{lin}). Additionally, the ripples caused by the buck converter will be attenuated and/or filtered by the linear Op-Amp. The smooth transition between the switching stage and the linear stage is realized by a hysteretic current feedback control. The hysteretic current feedback control consists of a current sensing resistor R_{sense} that senses the output current of the linear stage and a hysteresis comparator to control the buck converter. The value of the sensing resistor R_{sense} is chosen to be $1\ \Omega$ in this case, as it needs to be much smaller than R_{load} (i.e., the load impedance presented by the PA) to achieve high efficiency.

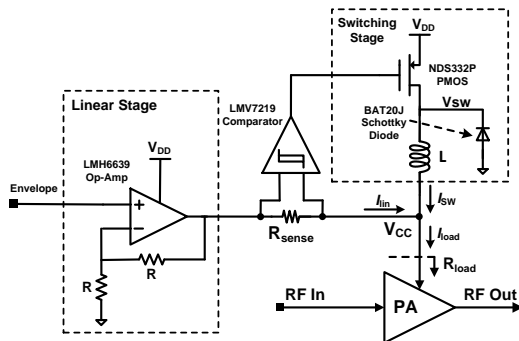


Fig. 4 Schematic of the linear-assisted switching envelope modulator (EM) designed by using COTS components

C. Efficiency and Nonlinearities of Envelope Modulator

Although many reported on the efficiency of the EM design in the literature [1] [2] [4] [13], its linearity and switching noise trade-offs vs. efficiency have not been studied as rigorously, which are especially critical for wideband signals. In this section, the nonlinearities of the discrete linear-assisted switching EM will be characterized. The switching noise and the bandwidth of the EM are two major factors that cause distortions to the output envelope signal. Understanding the effects of the switching frequency and bandwidth limitation of the EM helps to optimize both efficiency and linearity of the overall ET-PA.

1) Bandwidth of the Envelope Modulator

Previous works suggest that for a good linearity performance, the linear stage (i.e., the Op-Amp) should have sufficient bandwidth to track the high frequency contents of the envelope signal with high fidelity [1] [4] [5]. In addition, once the linear Op-Amp stage is used to assist the switching buck converter, it should have sufficient

bandwidth to suppress the switching ripples/noise. The switching ripples beyond the bandwidth of the linear stage can distort the envelope signal, and be mixed with the modulated carrier in the PA to cause large spurious noise at the PA output, potentially degrading the system linearity.

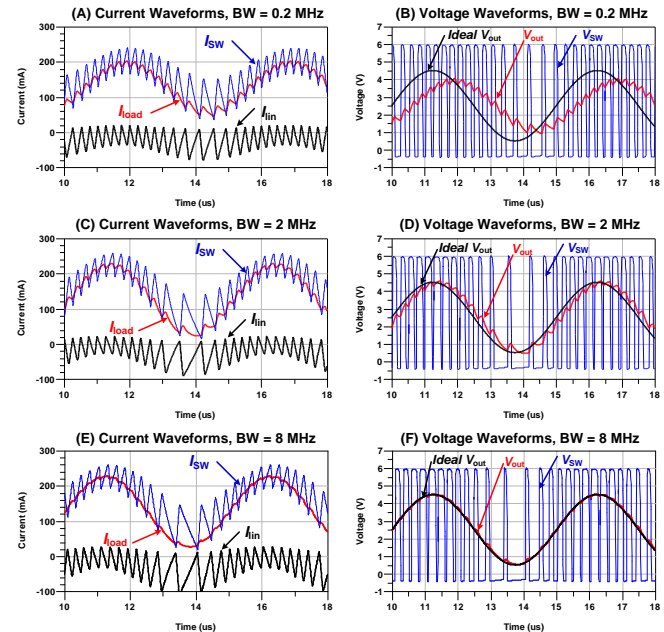


Fig. 5 Simulated (A, C, E) current and (B, D, F) voltage waveforms of the EM; the behavior model is used for the Op-Amp with different 1-dB bandwidths, while realistic SPICE models are used for other blocks of the EM. Input voltage = $1.25 + \sin(2\pi \cdot 200\text{kHz} \cdot t)$ V, $L = 4.7\ \mu\text{H}$, $R_{load} = 20\ \Omega$.

To investigate the effect of the EM bandwidth, the commercial available Op-Amp (i.e., LMH6639 in Fig 4) is replaced with an Op-Amp behavior model provided by Agilent's ADS, such that the bandwidth of the Op-Amp can be changed manually in the SPICE simulations. The realistic SPICE models are still used for other blocks of the EM. Fig. 5 shows the simulated current and voltage waveforms of the EM using different 1-dB bandwidths of the Op-Amp at an input wave of $1.25 + \sin(2\pi \cdot 200\text{kHz} \cdot t)$ V. Here, the 1-dB bandwidth is defined as the frequency where the gain response decreases by 1 dB. As shown in Fig. 5(A), (C) and (E), the output current of the switching stage (I_{SW}) has large ripples on the waveforms, which need to be suppressed or cancelled by the output current of the linear stage (I_{lin}) to reproduce an accurate load current waveform (I_{load}). When the 1-dB bandwidth of the Op-Amp is set as 0.2 MHz, the output voltage (V_{out}) of the EM exhibits not only the switching ripples but also with some attenuation (Fig. 5(B)). When the 1-dB bandwidth of the Op-Amp is set as 2 MHz, the output voltage waveform V_{out} can follow the input voltage without attenuation, but the switching ripples still cannot be suppressed (Fig. 5(D)). When the 1-dB bandwidth of the Op-Amp is set as 8 MHz, V_{out} can now follow the input voltage with high fidelity and at a low noise level (Fig. 5(F)).

To further demonstrate the importance of having a wideband linear stage in the EM to meet the stringent

linearity specs, the entire ET-PA using the monolithic SiGe PA is simulated with the RF/analog/digital co-simulation bench. The behavior model is used for the Op-Amp, while the realistic SPICE models are used for the PA and the other blocks of the EM. The inductor (L) of the buck converter is first chosen around 40 μH . The effect of the value of L on the EM design will be discussed in the next section. The simulated output error-vector-magnitude (EVM) values of the ET-PA against different 1-dB bandwidths of the Op-Amp stage are plotted in Fig. 6 for the WiMAX 64QAM 8.75 MHz signal. As shown in Fig. 6, the EVM values of the ET-PA decrease as the 1-dB bandwidth of the Op-Amp increases, and become saturated to $\sim 1.8\%$ after the 1-dB bandwidth of the Op-Amp becomes larger than 18 MHz. Fig. 7 shows the simulated transmission output spectra of the ET-PA with different bandwidths of the Op-Amp. There is a large improvement on the Adjacent Channel Power Ratio (ACPR) when the 1-dB bandwidth of the Op-Amp increases from 8 MHz to 18 MHz, enabling the output spectrum passing the stringent WiMAX spectral mask specs for the case of 18 MHz. As indicated by Figs. 6-7, the required bandwidth of the EM for the ET-PA needs to be able to respond to the envelope frequency contents to at least 2x of the original instantaneous signal bandwidth.

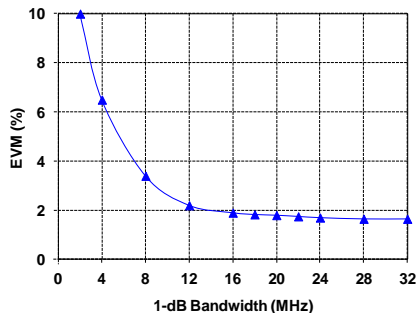


Fig. 6 Simulated output EVM of the ET-PA vs. 1-dB bandwidth of the Op-Amp for the WiMAX 64QAM 8.75 MHz signal. The behavior model is used for the Op-Amp, while realistic SPICE models are used for the SiGe PA and other blocks of the EM $P_{in} = 6 \text{ dBm}$, $P_{out} = 16 \text{ dBm}$.

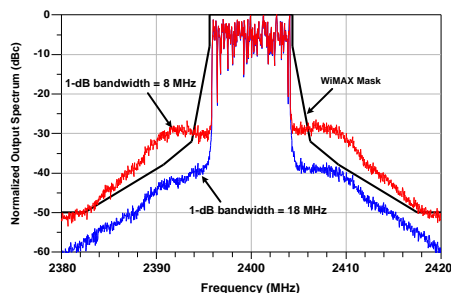


Fig. 7 Simulated output spectra of the ET-PA using different bandwidths of Op-Amp for the WiMAX 64QAM 8.75 MHz signal. The behavior model is used for the Op-Amp, while realistic SPICE models are used for the SiGe PA and other blocks of the envelope modulator. $P_{in} = 6 \text{ dBm}$, $P_{out} = 16 \text{ dBm}$.

2) Switching Frequency of Envelope Modulator

The average switching frequency of the EM shown in Fig. 4 is well analyzed in [4] and can be expressed as:

$$f_{switch} = \frac{R_{sense}}{L} \cdot \frac{V_{DD}}{2h} D \left(1 - D \cdot \frac{V_{rms}^2}{V_{dc}^2} \right) = \frac{R_{sense}}{L} \cdot \frac{V_{dc}}{2h} \left(1 - \frac{V_{rms}^2}{V_{DD} \cdot V_{dc}} \right) \quad (3)$$

, where V_{dc} and V_{rms} are the average and root-mean-square voltages of the output envelope signal, respectively; h is the hysteresis voltage of the comparator, and D is the duty ratio that can be calculated from V_{dc}/V_{DD} . In this design, the comparator LMV7219 has a predetermined internal hysteresis h of 7-10 mV according to the data sheet and the SPICE simulations. Therefore, from (3) the average switching frequency can now be mainly controlled by the value of L . The drawback of using a small L is that it usually generates more switching ripples at high frequencies, making the design of the linear stage more challenging [11].

Fig. 8 shows the SPICE simulated waveforms and spectra of the EM designed using two different values of L with an input waveform of $1.25 + \sin(2\pi \cdot 500\text{kHz} \cdot t) \text{ V}$. This time, the realistic SPICE models are used for all blocks of the EM simulations. The switching current I_{sw} supplies both DC and AC components of the load current (I_{load}) by using an L of 4.7 μH ; a higher switching frequency and large switching ripples on the waveform of I_{sw} can be observed from Fig. 8(A). Such large switching ripples need to be suppressed or cancelled by the output current of the linear Op-Amp (I_{lin}), which can be clearly shown by the spectra of I_{sw} and I_{load} in Figs. 8(E) and (G). On the other hand, for the case of $L = 68 \mu\text{H}$, I_{sw} supplies only the DC component of I_{load} , while the AC component is taken care of by the linear Op-Amp, as shown in Fig. 8(B). Also, the spectra of I_{sw} and I_{load} for the case of $L = 68 \mu\text{H}$ have smaller harmonics than those using $L = 4.7 \mu\text{H}$. These SPICE simulations indicate that the optimal value of L should be selected according to the best trade-off of maximum efficiency and linearity.

Fig. 9 shows the SPICE simulated efficiency of the EM and the EVM of the ET-PA using the monolithic SiGe PA presented in Fig. 1. The realistic SPICE models are used for the SiGe PA and all blocks of the EM. From the pure view point of efficiency, the optimal value of L for the best efficiency is 8.2 μH . Smaller L results in higher switching frequency that can cause significant switching loss and ripples. On the other hand, too large of the L makes the buck-converter only able to supply the DC component of the load current, and in that case the lower efficiency Op-Amp has to deliver the remaining AC contents (as illustrated in Fig. 8 (B)), leading to lower efficiency for the EM and thus the overall ET-PA system. Rather large L can also cause high parasitic resistance to decrease its efficiency. In addition, as shown in Fig. 9, the output EVM of the ET-PA is increased (i.e., linearity degraded) as L decreases. For example, the efficiency of the EM is increased by 4% by reducing L from 100 μH to 8.2 μH , but at the slight cost of worse EVM from 2.45% to 2.8%.

Fig. 10 shows the SPICE simulated output spectra of the ET-PA using L of 8.2 μH and L of 27 μH , respectively. When the larger L (27 μH) is chosen, the ACPR is 4-6 dB better at the offset of 5-8 MHz from the center frequency. Please note the output spectrum for the case of $L = 8.2 \mu\text{H}$ slightly violates the WiMAX spectral mask.

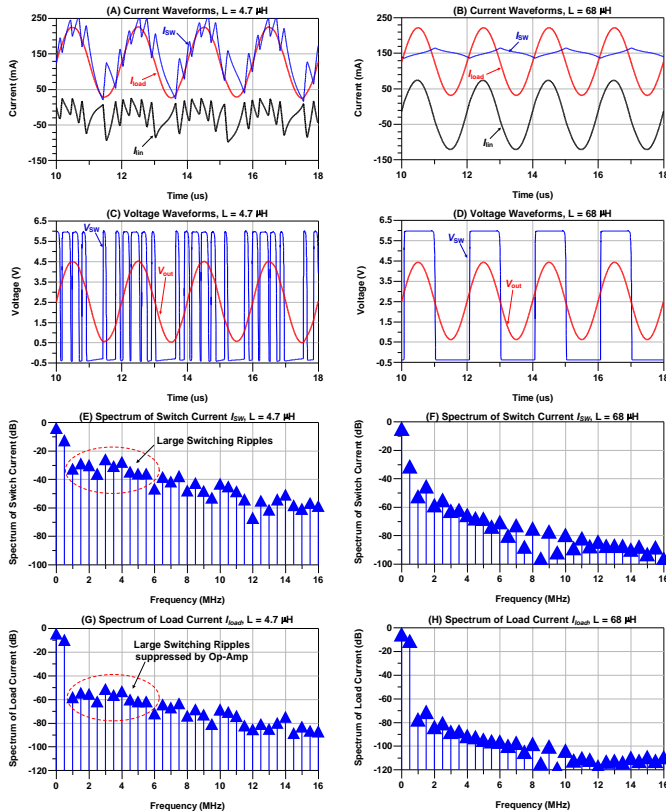


Fig. 8 SPICE simulated (A, B) current waveforms, (C, D) voltage waveforms, (E, F) spectra of the switching current I_{SW} , and (G, H) spectra of the output load current I_{load} of the EM using two different values of L ($4.7 \mu\text{H}$ vs. $68 \mu\text{H}$). The realistic SPICE models are used for the envelope modulator. $R_{load} = 22 \Omega$, the input voltage = $1.25 + \sin(2\pi \cdot 500\text{kHz} \cdot t)$ V.

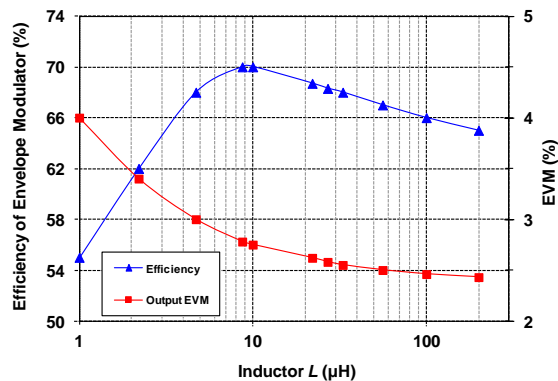


Fig. 9 SPICE simulated efficiency of the EM and output EVM of the ET-PA using different values of L for WiMAX 64QAM 8.75MHz signal. Realistic SPICE models were used for the PA and EM. $V_{DD} = 4.2$ V, $P_{out} = 17$ dBm.

Figs. 9-10 indicate that a small efficiency improvement may not be worthwhile if one has to sacrifice the linearity of overall ET-PA. Therefore, the L of $27 \mu\text{H}$ is chosen in the design for our EM to achieve best trade-off of efficiency vs. linearity, which is of course dependent on the best high-Q inductor available with the given budget. Fig. 11 shows the measured efficiency of the EM with different bandwidths of the WiMAX 64QAM signals. Note the efficiency of the EM shown here is only reduced by 2.5% when the signal bandwidth increased from 1.5 MHz to 20 MHz.

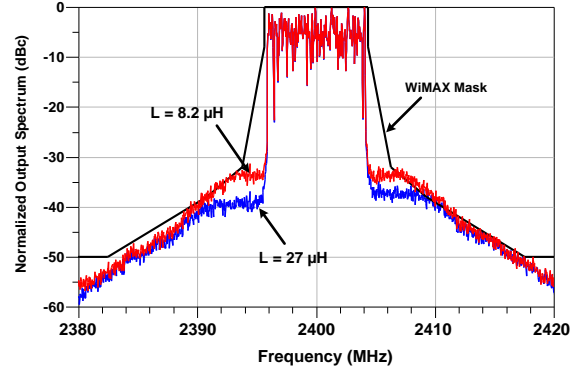


Fig. 10 Simulated output spectra of the ET-PA using different values of L for the WiMAX 64QAM 8.75 MHz signal. Realistic SPICE models were used for the SiGe PA and the EM. $V_{DD} = 4.2$ V, $P_{out} = 17$ dBm.

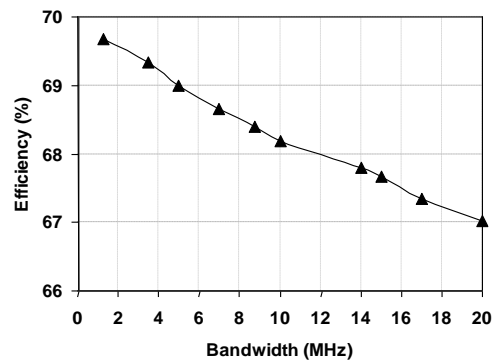


Fig. 11 Measured efficiency of the EM for different bandwidths of WiMAX 64QAM signals; $V_{DD} = 4.2$ V, $R_{load} = 22 \Omega$, average output voltage = 2.3 V.

When the output current is low, the inductor may be completely discharged at the “OFF” state of the buck converter before the switcher is turned on again, which is often called as the “discontinuous mode” for DC-DC converter design [22]. Therefore, another concern in the selection of the inductor value is to ensure the buck converter does not go into the discontinuous mode operation [22]. The boundary of the discontinuous mode occurs at where the output DC current (I_o) equals to one half of the peak-to-peak inductor ramp current ΔI (i.e., $0.5\Delta I = I_o$). For the stand-alone buck converter controlled by the conventional pulse-width modulation (PWM) scheme, the minimal L should be determined to avoid the discontinuous mode at the minimum DC output current ($I_{o,min}$) as [22]

$$L_{min} = \frac{(V_{DD} - V_{out,DC}) \cdot D}{\Delta I \cdot f_{SW}} = \frac{(V_{DD} - V_{out,DC}) \cdot V_{out,DC}}{2I_{o,min} \cdot f_{SW} \cdot V_{DD}} \quad (4)$$

, where $V_{out,DC}$ is the output DC voltage, D is the duty cycle, and f_{SW} is the switching frequency determined by the PWM control scheme. For example, if the EM were to be implemented using the conventional PWM control scheme for this ET-PA, one could obtain the $V_{out,DC} = 2.3$ V, $I_{o,min} = 33$ mA (i.e., at $R_{load} = 70 \Omega$ presented by the SiGe PA as shown in Fig. 2). Therefore, the minimal inductor value calculated based on (4) would be $\sim 16 \mu\text{H}$ for a PWM-controlled buck-converter, assuming $f_{SW} = 1$ MHz.

However, for the linear-assisted switching EM design presented here, the peak-to-peak inductor ramp current ΔI is limited under $2h/R_{\text{sense}}$, which is not related with the inductor value [4]. This is because once the switching current I_{sw} is h/R_{sense} lower than the load current I_{load} , the hysteresis comparator will immediately sense the current difference and turn on the switcher again, assuming the switcher can response fast enough [4]. In the practical design, however, the switcher is not ideal due to its intrinsic gate capacitance and resistance, therefore it may not respond fast enough with a high switching frequency, and this frequency is directly determined by the inductor value. Also, the hysteresis window h increases with higher input slew rate [23]. The SPICE simulations show that h is ~ 7 mV with the input voltage ramp below 0.2 V/ μ s, but increases to ~ 43 mV with the input voltage ramp of 4 V/ μ s. According to the simulation, the minimal L is 1.2 μ H to avoid the discontinuous mode operation for this EM design. Fig. 12 shows the SPICE simulated current waveforms of the linear-assisted EM at the boundary of the discontinuous mode. Depending on the accuracy of the device modeling and the packaging parasitic, the inductance in the practical implementation may be lower than the simulated value.

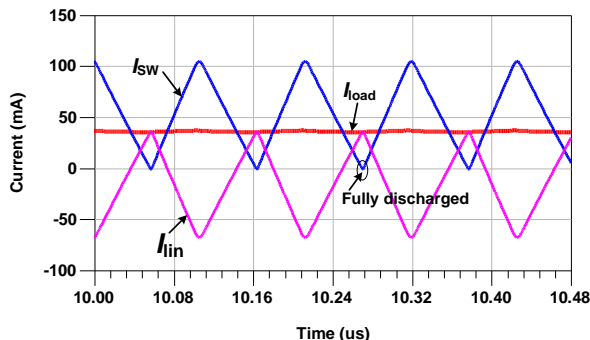


Fig. 12 SPICE simulated current waveforms of the discrete linear-assisted switching EM at the boundary of the discontinuous mode ($L = 1.2$ μ H)

III. EXPERIMENTAL RESULTS OF THE SiGe ET-PA

A. Efficiency and Linearity of the Stand-Alone PA

First, the stand-alone PA with fixed-supply voltage is tested to serve as a reference for the comparison with the ET-PA. Fig. 13 shows the measured gain, PAE and EVM vs. P_{out} for the WiMAX 64QAM 8.75 MHz signal (PAR = 10.5 dB) at 2.3 GHz. Without using any off-chip matching elements, the PAE of the SiGe PA reached 39% at the P_{out} of 17.8 dBm, but with a rather high output EVM of 11.7% (the EVM spec of WiMAX 64QAM is 5.0% or -26 dB). At P_{out} of 16 dBm, the stand-alone PA already violates the lenient EVM spec. Increasing V_{CC} could reduce the EVM as shown in Fig. 14, but at the cost of lower efficiency.

B. Efficiency and Linearity of the ET-PA

The discrete EM discussed earlier is used to modulate the supply voltage V_{CC} of the PA to form an ET-PA system. Please note that no predistortion is used in this work. The entire ET-PA operates at V_{DD} of 4.2 V. Fig. 15 shows the measured EVM, gain and overall PAE vs. P_{out} of the ET-PA.

Note the overall PAE (or the ET-PA composite PAE) includes the power consumption of the EM. The overall PAE is 30.5% at P_{out} of 17 dBm with an EVM of 4.4%. Judging from the PAE of $\sim 50\%$ for the SiGe PA at P_{out} of 17 dBm (Fig. 2) and the efficiency of the EM of $\sim 68\%$ (Fig. 11), the expected overall efficiency of the ET-PA would be 34%, which is close to the measured data observed from Fig. 15.

Fig. 16 shows the output spectra of the ET-PA and the stand-alone PA with fixed supply. At the same P_{out} of 17 dBm, the ET-PA successfully passes the stringent WiMAX 64QAM mask defined by European Telecommunications Standards Institute (ETSI), while the stand-alone PA fails the spectral mask badly. The ET-PA operates at its $P_{2\text{dB}}$ point for P_{out} of 17 dBm, but still impressively passes the WiMAX emission mask. The better linearity of the ET-PA is probably due to the same envelope shaping function applied in the system as [24], which linearizes the AM-AM of the ET-PA across the instantaneous P_{out} range. Fig. 17 further shows that the maximum linear P_{out} of the fixed-supply PA is only ~ 13.5 dBm in order to pass the WiMAX spectral mask, leading to a PAE of only $\sim 26\%$. Therefore, the ET-PA outperforms the fixed-supply PA by 3.5 dB on maximum linear P_{out} and 4.5% on PAE. Table I summarizes the performances of our ET-PA and its comparison with other state-of-the-art polar/ET-PAs.

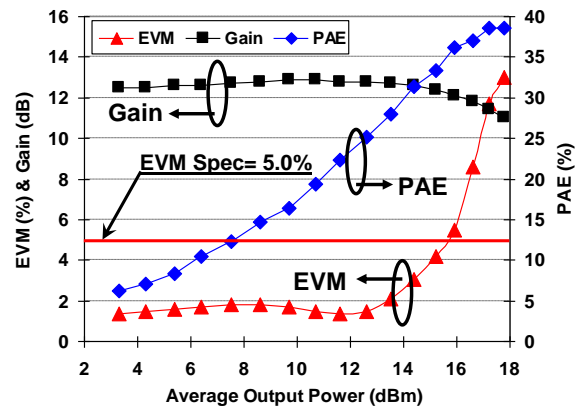


Fig. 13 Measured EVM, gain and PAE vs. average P_{out} of the stand-alone SiGe PA at V_{CC} of 3.6 V for WiMAX 64QAM 8.75MHz signal at 2.3 GHz.

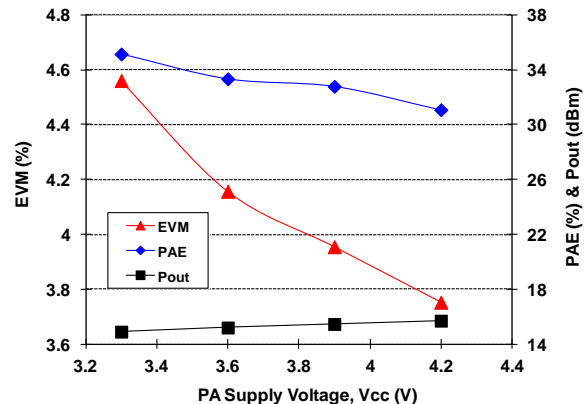


Fig. 14 Measured EVM, PAE and P_{out} vs. V_{CC} of the stand-alone PA for the WiMAX 64QAM 8.75 MHz signal at 2.3 GHz. $P_{\text{in}} = 3$ dBm

TABLE I. PERFORMANCE SUMMARY AND COMPARISON OF OUR ET-PA WITH STATE-OF-THE-ART ET OR POLAR PAs

	Freq. (GHz)	Gain (dB)	⁽¹⁾ P _{out} (dBm)	Overall PAE	EVM	EM Efficiency	Signal BW (MHz)	Modulation	⁽²⁾ PD	Technology
[1]	0.9	8.41	20.41	44.4%	6.0%	65%	0.384	EDGE	No	PA: 0.18μm SiGe BiCMOS EM: discrete COTS
[4]	2.4	6.5	19	28%	2.8%	60%	20	WLAN 64QAM	Yes	Discrete COTS
[6]	1.75	---	23.8	22%	1.69%	---	0.384	EDGE	Yes	0.18μm CMOS
[10]	1.88	27.9	23.9	34.3%	2.98%	75%	5	WiMAX 64QAM	No	PA: 2μm InGaP/GaAs EM: 0.13μm CMOS
[17]	2.0	---	19.6	22.6%	2.5%	---	20	WLAN 64QAM	No	0.13μm CMOS
[18]	2.4	11	20	28%	5%	65%	20	WLAN 64QAM	Yes	0.18μm SiGe BiCMOS
[19]	1.56	---	14.7	8.9%	4.6%	---	20	WLAN 64QAM	No	0.18μm CMOS
[20]	1.92	---	15.3	22%	1.5%	---	5	WiMAX 64QAM	Yes	0.13μm SOI-CMOS
This work	2.3	10.5	17.0	30.5%	4.4%	69%	8.75	WiMAX 64QAM	No	PA: 0.18μm SiGe BiCMOS EM: discrete COTS

Note:

- (1) P_{out}: The maximum linear P_{out} that passes the linearity specs of the specific wireless standard.
- (2) PD: Predistortion
- (3) [1] [4] [10] [18] proposed ET-PAs, [6] [17] proposed polar PAs, and [19] [20] proposed digitally modulated polar PAs.

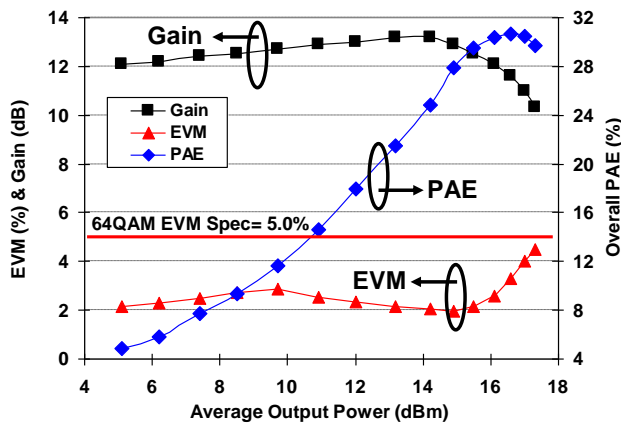


Fig. 15 Measured EVM, gain and overall PAE vs. P_{out} of the ET-PA system for the WiMAX 64QAM 8.75 MHz signal at 2.3 GHz; V_{DD} = 4.2 V

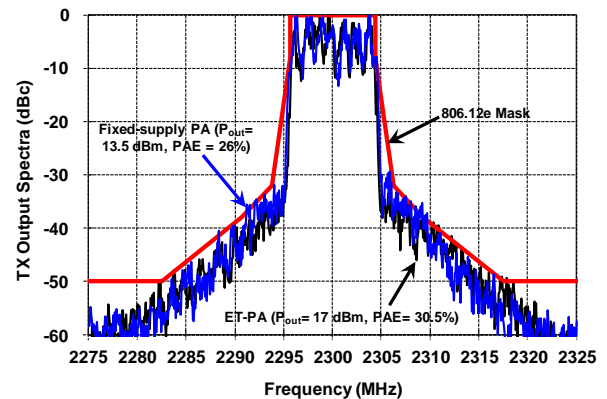


Fig. 17 Measured output spectra of the ET-PA (P_{out}=17 dBm) and fixed-supply PA (P_{out}=13.5 dBm) for WiMAX 64QAM 8.75 MHz at 2.3 GHz.

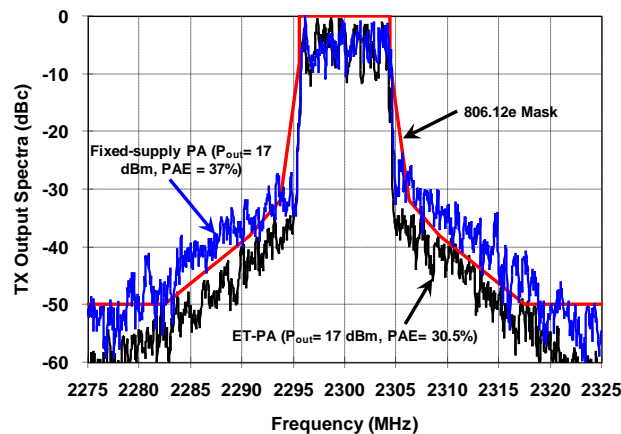


Fig. 16 Measured output spectra of the ET-PA and fixed-supply PA for WiMAX 64QAM 8.75 MHz at 2.3 GHz. P_{out} kept at 17 dBm for both cases.

IV. CONCLUSION

The circuits and system design insights of a high efficiency and linear ET-PA system have been discussed using a SiGe PA and a discrete linear-assisted switching EM. The switching frequency of the switching stage and the bandwidth of the linear stage have been studied carefully to make the EM suitable for high PAR wideband applications. The WiMAX 64QAM 8.75 MHz signal was used to characterize the linearity and efficiency performances of the ET-PA system. Without needing any predistortion, the entire ET-PA system achieved an overall PAE of 30.5% at P_{out} of 17 dBm with an EVM of 4.4%, while successfully passing the stringent WiMAX spectral mask.

ACKNOWLEDGMENT

The authors like to thank Dr. K.-S. Lu, CEO of Diodes Inc., Plano, TX, for generously donating the Keh-Shew Lu Regents Endowment Fund at Texas Tech University (TTU).

We also like to acknowledge of the funding support from Texas Instruments (TI) and other companies.

REFERENCES

- [1] J. Lopez *et al.*, "Design of highly efficient wideband RF polar transmitter using the envelope-tracking technique," *IEEE J. Solid-State Circuits*, vol. 44, no. 9, pp. 2276-2294, Sept., 2009.
- [2] Y. Li *et al.*, "A Highly Efficient SiGe Envelope-Tracking Power Amplifier with an Integrated CMOS Envelope Modulator for Mobile WiMAX/3GPP LTE Transmitters," *IEEE Trans. Microw. Theory Tech.*, vol. 59, no. 10, pp. 2525-2536, Oct. 2011.
- [3] D. Y.C. Lie *et al.*, "Highly-efficient monolithic class E SiGe power amplifier design at 900 and 2400MHz," *IEEE Trans. Circuits Syst. I – Reg. Papers*, vol. 56, no. 7, pp. 1455-1466, July 2009.
- [4] F. Wang *et al.*, "An improved power-added efficiency 19-dBm hybrid envelope elimination and restoration power amplifier for 802.11g WLAN application," *IEEE Trans. Microw. Theory Tech.*, vol. 54, no. 12, pp. 4086-4099, Dec. 2006.
- [5] B. J. Minnis, P. A. Moore, P. N. Whatmough, P. G. Blanken, and M. P. van der Heijden, "System-efficiency analysis of power amplifier supply-tracking regimes in mobile transmitters," *IEEE Trans. Circuits Syst. I – Reg. Paper*, 56, 1, pp. 268-279, Jan. 2009.
- [6] P. Reynaert and M. S.J. Steyaert, "A 1.75-GHz polar modulated CMOS RF power amplifier for GSM-EDGE," *IEEE J. Solid-State Circuits*, vol. 40, no. 12, pp. 2598-2608, Dec. 2005.
- [7] D. K. Su and W. J. McFarland, "An IC for linearizing RF power amplifier using envelope elimination and restoration," *IEEE J. Solid-State Circuits*, vol. 33, no. 12, pp. 2252-2258, Dec. 1998.
- [8] V. Pinon, F. Hasbani, A. Giry, D. Pache, and C. Garnier, "A single-chip WCDMA envelope reconstruction LDMOS PA with 130 MHz switched-mode power supply," *IEEE Int. Solid-State Circuits Conf. Dig. Tech. Papers*, Feb. 2008, pp. 564-565.
- [9] J. Kitchen, W. Chu, I. Deligoz, S. Kiaei, and B. Bakkaloglu, "Combined linear and Δ -modulated switch-mode PA supply modulator for polar transmitters," *IEEE Int. Solid-State Circuits Conf. Tech. Dig.*, Feb. 2007, pp. 82-83.
- [10] J. Choi, D. Kim, D. Kang, and B. Kim, "A polar transmitter with CMOS programmable hysteretic-controlled hybrid switching supply modulator for multistandard applications," *IEEE Trans. Microw. Theory Tech.*, vol. 57, no.7, pp. 1675-1686, July 2009.
- [11] R. Shrestha, R. v.d. Zee, A. d. Graauw, and B. Nauta, "A wideband supply modulator for 20 MHz RF bandwidth polar PAs in 65 nm CMOS," *IEEE J. Solid-State Circuits*, vol. 44, no. 4, pp. 1272-1280, Apr. 2009.
- [12] F. H. Raab, "Split-band modulator for Kahn-technique transmitters," *IEEE MTT-S Int. Microw. Symp. Dig.*, 2001, pp. 887-890.
- [13] M. Kwak *et al.*, "Design of a wideband high-voltage high-efficiency BiCMOS envelope amplifier for micro-base-station RF power amplifier," *IEEE Trans. Microw. Theory Tech.*, vol. 60, pp. 1850-1861, June 2012.
- [14] F. Wang, A. H. Yang, D. F. Kimball, L. E. Larson, and P. M. Asbeck, "Design of wide-bandwidth Envelope-Tracking power amplifiers for OFDM applications," *IEEE Tran. Microw. Theory Tech.*, vol. 53, no. 4, pp. 1244-1255, Apr. 2005.
- [15] M. Helaoui, S. Boumaiza, A. Chazel, and F. M. Ghannouchi, "On the RF/DSP design for efficiency of OFDM transmitters," *IEEE Trans. Microw. Theory Tech.*, 53, 7, pp. 2355-2361, 2005.
- [16] J. Jeong, D. F. Kimball, M. Kwak, C. Hsia, P. Draxler, and P. M. Asbeck, "Wideband envelope tracking power amplifiers with reduced bandwidth power supply waveforms and adaptive digital predistortion techniques," *IEEE Tran. Microw. Theory Tech.*, vol. 53, no. 4, pp. 1244-1255, Apr. 2005.
- [17] J. S. Walling, S. S. Taylor, and D. J. Allstot, "A class-G supply modulator and class-E PA in 130nm CMOS," *IEEE J. Solid-State Circuits*, vol. 44, no. 9, pp. 2339-2347, Sept. 2009.
- [18] F. Wang, D. Kimball, D. Y.C. Lie, P. Asbeck, and L. E. Larson, "A monolithic high-efficiency 2.4-GHz 20-dBm SiGe BiCMOS envelope-tracking OFDM power amplifier," *IEEE J. Solid-State Circuits*, vol. 42, no. 6, pp. 1271-1281, June 2007.
- [19] A. Kavousian, D. K. Su, M. Hekmat, A. Shirvani, and B. A. Wooley, "A digitally modulated polar CMOS power amplifier with a 20-MHz channel bandwidth," *IEEE J. Solid-State Circuits*, vol. 43, no. 10, pp. 2251-2258, Oct. 2008.
- [20] C. D. Presti, F. Carrara, A. Scuderi, P. M. Asbeck, and G. Palmisano, "A 25 dBm digitally modulated CMOS power amplifier for WCDMA/EDGE/OFDM with adaptive digital predistortion and efficient power control," *IEEE J. Solid-State Circuits*, vol. 44, no. 7, pp. 1883-1896, July 2009.
- [21] I. Kim, Y. Woo, J. Kim, J. Moon, J. Kim, and B. Kim, "High-efficiency hybrid EER transmitter using optimized power amplifier," *IEEE Trans. Microw. Theory Tech.*, vol. 56, no. 11, pp. 2582-2593, Nov. 2008.
- [22] A. I. Pressman, *Switching Power Supply Design*, Second Edition, New York, NY: McGraw Hill, 1998.
- [23] R. Gregorian, *Introduction to CMOS Op-Amps and Comparators*, New York, NY: Wiley, 1999.
- [24] Y. Li *et al.*, "Circuits and system design of RF polar transmitters using envelope-tracking and SiGe power amplifier for mobile WiMAX," *IEEE Trans. Circuits Syst. I – Reg. Papers*, vol. 58, no. 5, pp. 893-901, May 2011.